Pertanika J. Sci. & Technol. 27 (4): 2281 - 2304 (2019)

PERTANIKA JOURNALS

SCIENCE & TECHNOLOGY

Journal homepage: http://www.pertanika.upm.edu.my/

Spatial Pattern and Temporal Variability of Sea Level Anomaly and Geostrophic Current in the Eastern Indian Ocean from Satellite Altimetry

Julian Saputra[1,2]*, Jonson Lumban-Gaol[2], James Parlindungan Panjaitan[2] and Agus Saleh Atmadipoera[2]

[1]Graduate School of Marine Technology Program, Institut Pertanian Bogor, West Java 16128, Indonesia
[2]Department of Marine Science and Technology, Institut Pertanian Bogor, West Java 16128, Indonesia

ABSTRACT

The Eastern Indian Ocean has complex dynamic circulation systems affected by monsoonal wind circulation and climate variation. This research aimed to investigate the spatial and temporal variability of the sea level, and the geostrophic currents in the Eastern Indian Ocean using altimeter data. We used daily time series sea level anomaly data from 2004-2016 and applied time-series analysis of EOF. The highest four-modes were adopted. Both sea level anomaly and geostrophic zonal component had the sum of explained variance with 79.68% and 35.65%, respectively. The spatial pattern of the sea level anomaly showed dominant variability spread around the west coast of Sumatra and south coast of Java with positive and negative anomalies, as shown in first and second modes, while the third and the fourth mode did not show substantial spatial variability. The dominant temporal variation revealed semi-annual, annual and inter-annual periodicity. Furthermore, for the geostrophic zonal current, spatial pattern in the first to third modes showed high variability around the west coast of Sumatra and south coast of Java, while in the offshore region they showed positive-negative anomalies. In the fourth mode, the spatial pattern showed low variability. The dominant temporal variation revealed annual, semi-annual and inter-annual periodicity. Based on the spatial and temporal variation of the data, the variability in the study area might be associated with the dynamic of coastally trapped Kelvin wave, upwelling and an inter-annual anomaly of IOD and ENSO. It was also noticed that some patterns indicated as dynamic of SJC and SEC signals.

Keywords: Altimeter data, geostrophic zonal component, sea level anomaly, the Eastern Indian Ocean, time-series analysis EOF, variability

ARTICLE INFO

Article history:
Received: 16 January 2019
Accepted: 11 July 2019
Published: 21 October 2019

E-mail addresses:
julian.saputra75@gmail.com (Julian Saputra)
jonson_lumbangaol@yahoo.com (Jonson Lumban-Gaol)
jppanjaitan1@yahoo.com (James Parlindungan Panjaitan)
agus.itk@gmail.com (Agus Saleh Atmadipoera)
* Corresponding author

ISSN: 0128-7680
e-ISSN: 2231-8526

INTRODUCTION

Satellite altimetry has been developed comprehensively. The early ages on satellite altimetry history was the first launch of Skylab (1973-1974) that showed the capability of measuring geoid and oceanographic parameters. In 1978, the new generation of Seasat satellite was launched, making the improvement in quality of data, which was widely distributed to the scientists (Escudier et al., 2017). Long term altimeter missions were started when Topex/Poseidon (T/P) was launched in 1992 to the latest Jason 3 mission in 2016. They provided assimilation products to improve accuracy of altimeter data. The assimilation missions produced reliable spatial and temporal resolution data (AVISO, 2016).

The data describes sea level variation which is very useful for advanced analysis, such as to calculate the trend of sea level rise, to detect climate and weather, and to classify polar ice sheets (Fu & Cazenave, 2001; Mansawan et al., 2016; Rosmorduc et al., 2011). Understanding variability of sea level is very useful to predict potential fishing ground (Fitrianah et al., 2016; Lumban-Gaol et al., 2015; Syah et al., 2016). Sea level variability information can be used to detect gobal climate change e.g., Dipole Mode and El-Nino/La-Nina (Lim & Hendon, 2017; Syamsudin & Kaneko, 2013). Sea level data has been used widely to detect ocean dynamic, since it is directly related to ocean circulation such as geostrophic approximation (Fu & Cazenave, 2001; Le Traon, 2013). The understanding of geostrophic current is necessary, since the major currents of global ocean e.g., Gulf Stream, Kuroshio Current, and the Antartic Circumpolar Current are approximately included geostrophic current (Gill, 1982).

One of the data produced by satellite altimetry is Sea Level Anomaly (SLA) which plays a direct role in ocean circulation, especially geostrophic flow. Hence, geostrophic current variability can be derived from sea level topography (Joseph, 2014). Some research utilizing altimeter data had already been conducted. One of the first research using 3 months altimetric Seasat mission over the Antartic Circumpolar Current (AAC) was carried out by Fu and Chelton (1985). The result showed that the ACC circulation around the the Southern Ocean tended to be eastward acceleration. Another research was done by Susanto et al. (2001), predicted that sea level were related to the thermocline depth in the Indian Ocean. Sea level data from satellite altimetry had been extensively used to determine the dynamics and variability of the ocean, especially in a mesoscale region (Potemra & Lukas, 1999). One of the recent studies has been done by Syamsudin and Kaneko (2013). They used SLA to detect variability in the Eastern Indian Ocean (EIO) region. They found a lot of variability occurring in the EIO were influenced by phenomena such as El-Niño/La Niña, Indian Ocean Dipole (IOD) and regional monsoonal winds.

This research was conducted in the EIO, precisely at 100°E-120°E and 4°S-20°S (Figure 1). This area is fascinating because the variability that occurred are subjects to many influences e.g., wind stress anomaly, particularly the influence of monsoonal winds

(Schiller et al., 2009; Susanto et al., 2001; Wyrtki, 1961). Moreover, sea water flow in the EIO is also influenced by the Indonesian Throughflow (ITF) that passes through the Makassar Strait as its central passage (Gordon & Kamenkovich, 2010; Song et al., 2004; Susanto & Song, 2015). The annual cycle of ITF flow in the Makassar Strait is stronger in the southeast monsoon, July to September (Atmadipoera et al., 2016; Susanto et al., 2012). The circulation occurring in this region, besides ITF, is the South Java Current (SJC). It flows in the tropical Indian Ocean along Sumatra and Java coast, and move through the Savu Sea to reach Ombay Strait, which is one of the primary ITF pathways (Sprintall et al., 2009). Another circulation in the EIO is the South Equatorial Current (SEC). The SEC brings low salinity water which flowing westward, and recirculate in the East Gyral Current (EGC) circulating eastward (Bray et al., 1997; Feng & Wijffels, 2002; Meyers et al., 1995). During the semi-annual monsoon transition period (April-May and October-November), the westerly wind forcing generates Kelvin wave in the equator Indian Ocean and propagate eastward, forming Coastally Trapped Kelvin Wave (CTKW) along western Sumatra and southern Java coast (Clarke & Liu, 1993; Sprintall et al., 2000). Upwelling and downwelling process along these coasts may be affected by the waves (Susanto et al., 2001).

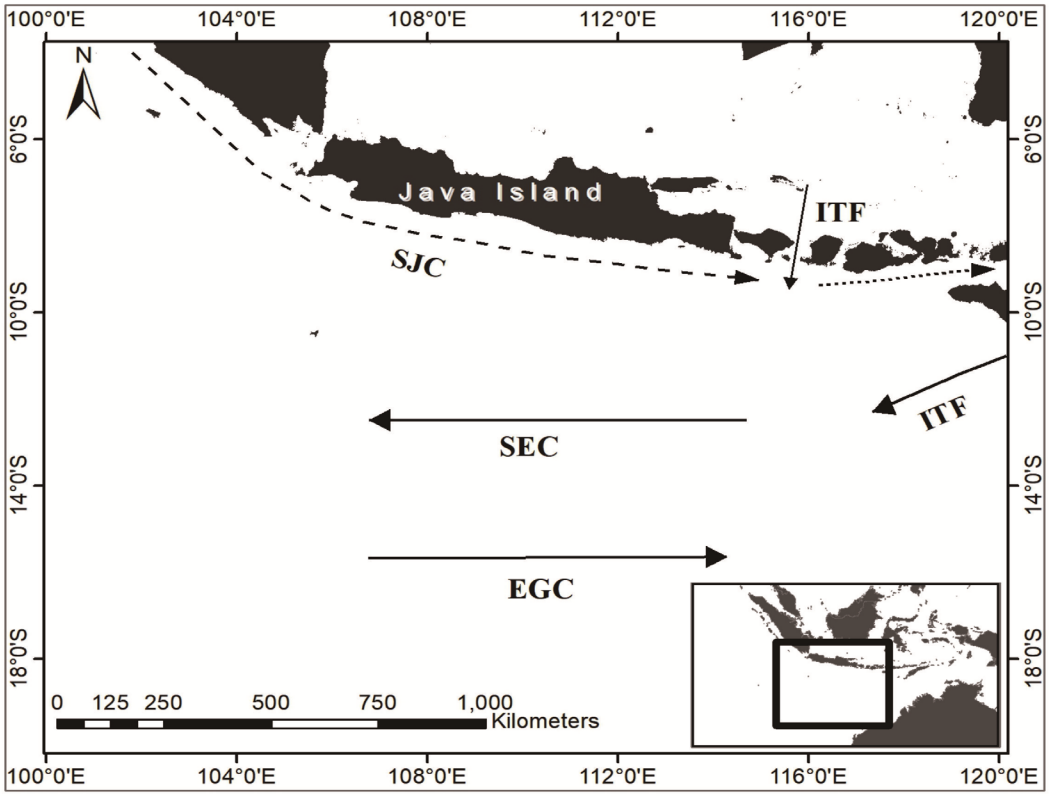

Figure 1. The surface current system in the EIO region. SEC: South Equatorial Current; SJC: South Java Current; EGC: Eastern Gyral Current; ITF: Indonesian Throughflow, adopted from Feng & Wijffels (2002) and Sprintall et al. (2010)

The interannual variability in the EIO region is prominently influenced by the IOD and El Niño-Southern Oscillation (ENSO) (Schott et al., 2009). The IOD is a pattern of internal variability in which sea surface temperature decreases in the eastern part of Indian Ocean, especially in the western coast of Sumatra, rising sea surface temperature in the western Indian Ocean region followed by high precipitation. The IOD occurs independently of the ENSO from the Pacific Ocean. Nevertheless, there is a link between IOD and ENSO. Usually, a negative IOD phase is followed by El Niño; likewise in the opposite phase, positive IOD is formed, followed by La Niña (Izumo et al., 2010). The ENSO plays essential roles in other oceanographic phenomena, i.e., sea level variation. During El Niño, the negative values of SLA occur near the south coast of Java, and positive values around the offshore region. The opposite situation occurs during La Niña, where the SLA values near the south coast of Java show positive values, while the offshore area has negative values (Syamsuddin et al., 2013).

Regarding the width of the coverage area, altimeter data is reliable for mesoscale studies, in which it has been constrained when utilizing in-situ data or model simulation. The limitation of using in-situ data is related to small area coverage, while model simulation results must be enhanced by validation (Fang et al., 2006). Considering the dynamic oceanographic processes and external influences from the Pacific Ocean and the effects of wind circulation in the Indian Ocean waters, the EIO region is very interesting for investigations. However, the collection of in-situ spatio-temporal data is challenging. Another challenge in using the model simulation is a validation procedure. Therefore, SLA data was utilized to produce variability in the EIO region. The purposes of this study were to investigate the spatial and temporal of SLA and geostrophic zonal current variability.

METHODS

The Data

The SLA data from satellite altimetry was used to meet the objectives of this study. The data was acquired in spatio-temporal form, better known as Delayed Time (DT) Mean Sea Surface Anomaly (MLSA). It is the integrated results of all altimeter missions such as HY-2A, Saral/AltiKa, Cryostat-2, Jason-1, Jason-2, T/P, Envisat, GFO, and ERS1/2. All the data from various missions were collected by *Segment Sol multimissions d'ALTimétrie, d'Orbitographie et de locali sation précise*/Data Unification and Altimeter Combination System (SSALTO/DUACS) (AVISO, 2016). Data could be downloaded on Copernicus Marine Environment Monitoring Service website (CMEMS http://marine.copernicus.eu/). The data spanning was 2004-2016 with daily temporal resolution. The SLA data was in gridded form with 0.25°x0.25° and was available in global coverage. The data coverage was 100°E-120°E and 4°S-20°S with the number of grids were 81x61, and 4749 layers representing time-series dimension.

Data preparation

The SLA data was available in global coverage. Cropping process was applied to achieve data in the EIO region only. The calculation in Stewart (2008) was followed to achieve geostrophic components. The surface geostrophic current estimation were calculated from the difference in water slope causing pressure differences. The zonal (u) and meridional (v) current components were obtained from the oceanic topographic gradient, gravitational force, and coriolis force. If it is assumed that density *(ρ)* and gravity (g) are constant at surface level, then geostrophic components can be calculated :

$$u = -\frac{g}{f}\frac{\partial \zeta}{\partial y};\ v = \frac{g}{f}\frac{\partial \zeta}{\partial x} \qquad (1)$$

where g is gravity, f is the coriolis force, and ζ is the sea level (Stewart 2008). The coriolis force equation can be written:

$$f = 2\Omega \sin \varphi \qquad (2)$$

where Ω is the angular velocity of the earth's rotation (rad/det), φ is the value of latitude.

The Coriolis force occurs due to the Earth's rotation, affecting the circulation into deflection to the right in the Northern Hemisphere and to the left in the Southern Hemisphere (Pond & Pickard, 1983; Tomczak & Godfrey, 2001). Although zonal and meridional current components were produced for geostrophic current, only zonal component was used in this study, because the dominant circulation in the EIO was west-east direction, as resulted from vector plot of geostrophic calculation derived from Conductivity, Temperature and Depth (CTD) data (Syamsudin & Kaneko, 2013).

Statistical process was applied to the data to determine the spatio-temporal mean and standard deviation of both on SLA data and geostrophic zonal component. The mean calculation was applied on SLA and geostrophic zonal component value of each grid, for all data both spatial and temporal. Meanwhile, the standard deviation was calculated by applying root-squared variance. After statistical processing, the climatological mean of SLA and geostrophic zonal component were calculated. The climatological mean was applied by averaging all data in the same month for all years.

Empirical Orthogonal Function (EOF) Analysis

Spatio-temporal variability is difficult to understand due to large coverage area and long time series data. Therefore, some techniques were applied to discover extreme variability from massive data. The idea was to compress the data into smaller values containing independent information. This can be done by applying EOF analysis. EOFs are a method for partitioning varian from a spatial data set that is distributed in time series, and they have been widely used in oceanographic data processing (Liu & Weisberg, 2007; Thomson

& Emery, 2014). EOF calculation was documented entirely and explained by Hannachi (2004) and Björnsson & Venegas (1999).

The principle of EOF analysis which is carried out in Hannachi et al. (2007) is to obtain the spatial (s) and temporal composition (t) denoted as:

$$X(t,s) = \sum_{k=1}^{M} c_k(t)\, \mathrm{u}_k(s) \qquad (3)$$

where *M* is the number of modes resulting from the decomposition of spatial signals $\mathrm{u}_k(s)$ and expansion coefficients or temporal principal components $c_k(t)$. If $X(t,s)$ is applied to SLA data and geostrophic component data in gridded form, at time *t* and position *s*, then the discrete value t_i and grid position s_j can be written x_{ij} for $i = 1, \ldots, n$ and $j = 1, \ldots, p$. If written in the form of a matrix:

$$X = (x_1 x_2 x_3)^T = \begin{pmatrix} x_{11} & x_{12} & \cdots & x_{1p} \\ x_{21} & x_{22} & \cdots & x_{2p} \\ \vdots & \vdots & \vdots & \vdots \\ x_{n1} & x_{n2} & \cdots & x_{np} \end{pmatrix} \qquad (4)$$

where $x_t = (x_{t1}, x_{t2}, \ldots x_{tp})^T$ describes the space in time *t*.

The limitation of this analysis regarding to variability patterns given by this EOF depict standing oscillation. Some limitation of EOF is the difficulty of physical interpretation. To overcome this shortcoming, the EOF method was modified to be Rotated EOF (REOF). This technique is also known as factor analysis as a factor rotation and aims to obtain a simple structure (Björnsson & Venegas, 1999).

EOF analysis produces variations in spatial patterns with eigenvector, describing the spatial pattern at all time range, the percentage of explained variance with eigenvalue, describing the contribution of variability in certain mode, and the temporal variation of Principal Components (PC) explaining how spatial pattern varies with time. EOF processing was carried out on SLA and geostrophic zonal component data throughout 2004-2016 to determine spatial and temporal variability in that period. EOF analysis on climatological mean data was also applied to determine spatial and temporal variability in the annual cycle. To determine how many modes would be used describing the variability, Jolliffe (2002) explained that the threshold for taking the cumulative explained variance was about 80%. So the certain numbers of modes that had 80% of cumulative explained variance were considered to explain the major variability in the EIO.

Power Spectral Density (PSD) analysis

Time series analysis was applied to determine dominant temporal variability from EOF analysis. Thus, EOF temporal variation results were analyzed by looking at the spectrum of energy density, where energy is defined as units per time domains (Thomson & Emery,

2014). Spectral energy analysis is better known as PSD analysis. PSD analysis was carried out to determine the energy value of each current signal per frequency. From this analysis, the relatively high power peak was shown to describe a dominant variability fluctuation in a certain frequency. Blackman and Tuckey developed a popular method to calculate PSD (as cited in Trauth, 2014, p. 158). In this study, PSD was calculated by determining the Fourier component of PC from SLA and geostrophic zonal component data generated from EOF in daily time scale. It was done to find more details from complex temporal variability occurring in the study area. The PSD analysis was calculated by:

$$PSD = \frac{X^*_{xx}(f)X_{xx}(f)}{f_s} = \frac{|X_{xx}(f)|^2}{f_s} \quad (5)$$

where $X^*_{xx}(f)$ is a complex conjugation of Fourier transforms from the autocorrelation function $X_{xx}(f)$ and f_s is the sampling frequency. The significant frequencies in PSD analysis were known by applying 95% confidence interval. The equation was written as:

$$\frac{v\tilde{X}_{xx}(f)}{X^2_{1-\alpha/2.v}} < X_{xx}(f) < \frac{v\tilde{X}_{xx}(f)}{X^2_{\alpha/2.v}} \quad (6)$$

where $\tilde{X}_{xx}(f)$ is the raw estimate of the observed time series, $X_{xx}(f)$ is the true spectrum, $X^2_{1-\alpha/2.v}$ and $X^2_{\alpha/2.v}$ are chi-square variables with $(1-\alpha)100\%$ confidence (Thomson & Emery, 2014).

RESULTS AND DISCUSSION

Mean and Standard Deviation

Mean and the standard deviation were calculated in both SLA and geostrophic flow data (Figure 2). The mean calculation of spatio-temporal data in Figure 2a showed that the maximum SLA value was 0.08 m with red color indicator, while the lowest value was 0.038 m with dark blue color indicator. The highest value was located around the coast of the Java Island, while the lowest value spread along the southern region far from the coast, around 100°E-106°E and 14°S-18°S. The overlayed geostrophic flow showed some eddies. There were two cyclonic eddies discovered at lower sea level, one in the area with coordinates 105°E-108°E and 15°S-16°S, and another area with coordinate 113°E-115°E and 16°S-17°S. The high SLA value with some vortexs showed around south coast of Java i.e., the Sunda Strait and another area around 108°E-110°E and 7°S-8°S.

The vortex occured in the Sunda Strait was probably because of the sea water circulation from the Java Sea and the Indian Ocean off west Java. In the Java Sea, the water circulation flowed westward, then turn southwestward through the Sunda Strait. On the other side, sea currents from the Indian Ocean around the west coast of Sumatra flowed southeastward along the southern coast of Java. Due to the convergence of the current in the Sunda Strait,

it caused a vortex that occurred anticyclonically. Rahmawitri et al. (2016) said that sea water from the Java Sea flows to the Indian Ocean through the Sunda Strait in upper 5 m. The next vortex in 108°E-110°E and 7°S-8°S was downwelling phenomenon that happened caused of Kelvin wave and northwest monsoon.

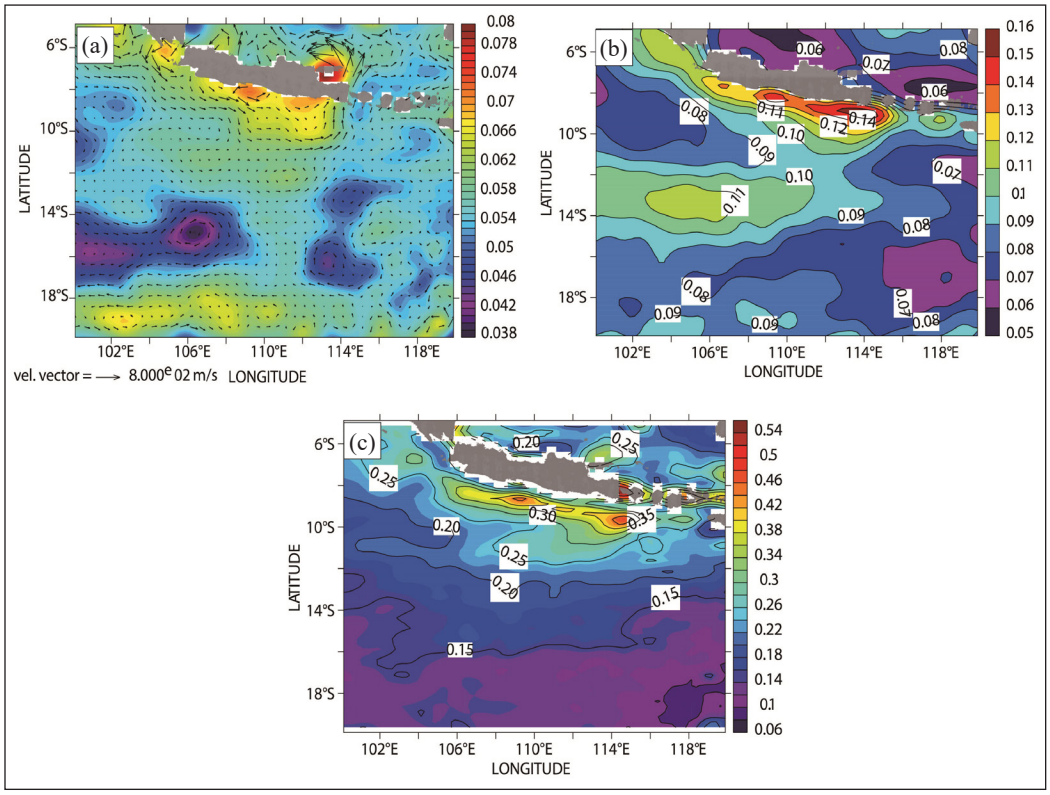

Figure 2. Mean and standard deviation of SLA and geostrophic current, (a) Mean of SLA and geostrophic current, (b) the standard deviation of SLA, (c) the standard deviation of geostrophic zonal component

The standard deviation of SLA data was presented in Figure 2b. In general, the higher standard deviation values were observed along west Sumatra and south Java coast, and around 10°S-15°S. However, in particular, the highest value was seen in the eastern part of south Java coast, precisely at 111°E-117°E and 8°S-11°S. It means that the highest difference of range from the average values were seen in that area. Meanwhile, the low standard deviations occurred at 114.5°E-120°E and 16°S-20°S. Furthermore, The geostrophic zonal component's standard deviations showed different aspects (Figure 2c). The higher standard deviations occurred along south Java coast, but the location was a little bit far from the coast. While the minimum values were mostly occurred at 14°S-18°S. The high number of standard deviations both in SLA and geostrophic zonal component near south coast of Java might be indicated as a high variability that occurred in that area.

Annual Cycle of SLA and Geostrophic Currents

The annual cycle of the SLA and geostrophic zonal component data were determined by applying EOF analysis of climatological mean data. This idea was generated from Fang et al., (2006). Spatial and temporal patterns were obtained with the two leading modes (Figure 3). The first mode accounted for 65.5% of the explained variance and the second mode accounted for 20.37% of the explained variance. The cumulative percentage of explained variance was 85.87%. In the first mode (Figure 3a), spatial patterns showed positive values in the lower part and negative values in the upper part of the study area. The centralization was seen near the south coast of Java, in the eastern part near Bali with the negative values. The different spatial patterns were shown in the second mode (Figure 3b), where there was a centralized spatial pattern with negative values at 111°E-118°E and 12°S-13°S. The PC graph of the first mode, presented in Figure 3c, described the temporal pattern showing the highest values occurring in August. Meanwhile, the PC graph of the second mode (Figure 3d) showed two positive peaks occurring in February and October, and one negative peak in May-June.

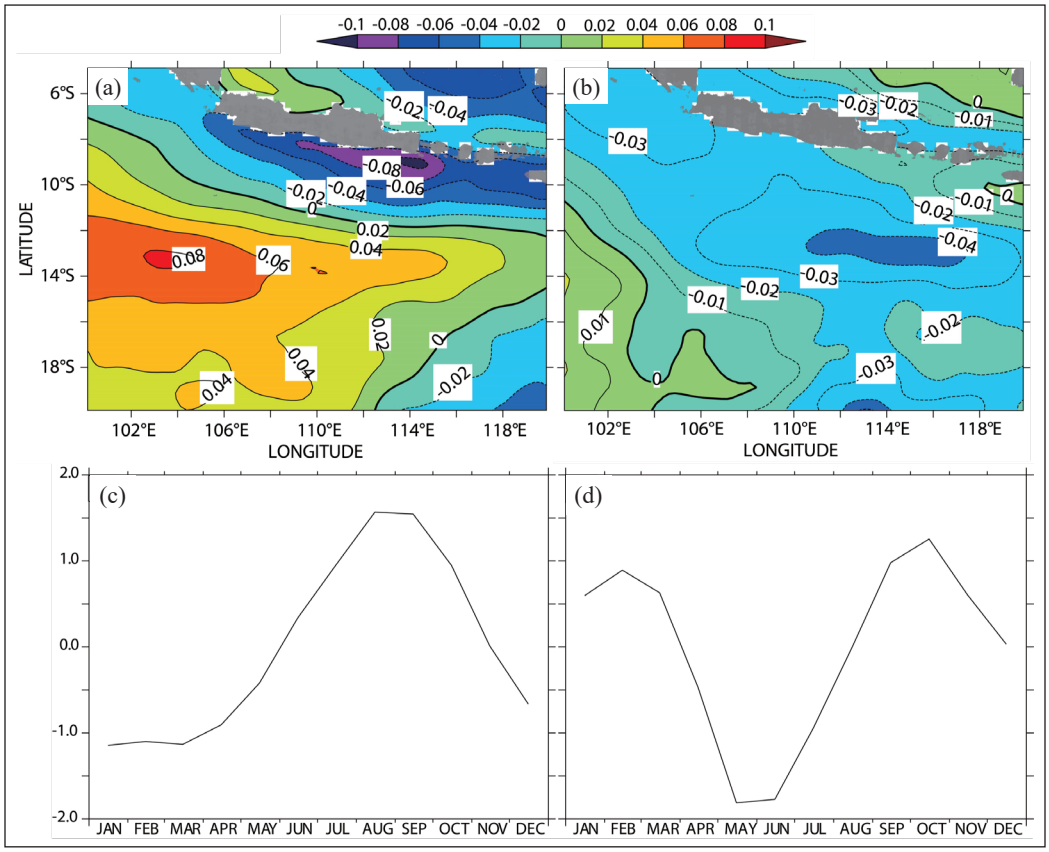

Figure 3. EOF analysis from SLA's climatological mean on two major modes, (a) spatial pattern the first mode, (b) spatial pattern the second mode, (c) PC graph of the first mode, (d) PC graph of the second mode

Annual cycle analysis of geostrophic zonal component was shown in the results of EOF processing on climatological mean. The results were displayed in two leading modes (Figure 4). The first mode accounted for 71.89% of the explained variance. The spatial pattern in the first mode (Figure 4a) showed negative values around the southern Java coast until 12°S, while the positive values distributed from 12°S to 20°S. Furthermore, in the second mode (Figure 4b) accounted for 9.74% of the explained variance, showing little variation with the positive values around the southern Java coast. Subsequently, in the temporal variation from the PC graph of the first mode (Figure 4c), the highest variability was seen in August and two negative peaks in January and December. Meanwhile, the temporal variation of the second mode from PC graph (Figure 4d) showed two positive peaks in May and November and two negative peaks in February and August.

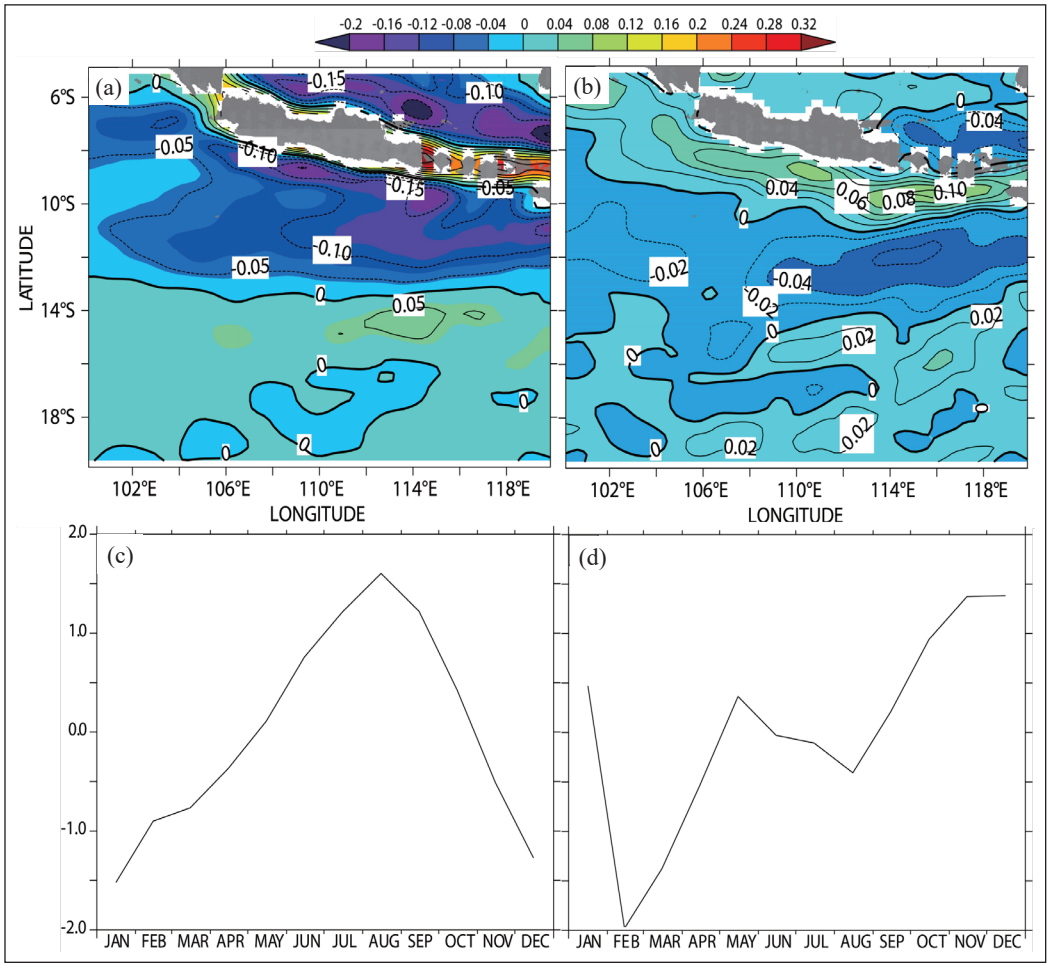

Figure 4. EOF analysis from the geostrophic zonal component's climatological mean on two major modes, (a) spatial pattern of the first mode, (b) spatial pattern the second mode, (c) PC graph of the first mode, (d) PC graph of the second mode

Variability of SLA and Geostrophic Zonal Component

The spatial and temporal SLA patterns were interpreted from the results of the EOF analysis in the EIO, displayed in the 4 biggest modes. The first mode (Figure 5) had the most substantial explained variance (52.31%). The spatial pattern showed positive values spread in the entire area. The highest values were seen along the west Sumatra and south Java coastz. The low eigenvector values formed a separate contour at remote locations from Java, which were pointed at 100°E-107°E and 10.5°S-16.5°S. In general, it was observed that the spatial pattern with high eigenvector values were located in the eastern part, while the low contour values were located in the western part of the study area (Figure 5a). The time series variation from PC was observed consistent oscillation's peak mostly happened in April, May, and November (Figure 5b). Furthermore, the energy fluctuations seen from PSD temporal analysis were revealed in the semi-annual (182 days), annual (356 days) and inter-annual (1024 days) periodicities (Figure 5c).

The different spatial pattern was shown in the second mode (Figure 6), accounting for 14.98% of the explained variance. The spatial pattern showed different phase oscillated in negative and positive values. The spatial pattern in this mode showed negative values along west Sumatra and south Java coast. A centered negative values located near the south of eastern Java were observed. The positive values spread in the southern part of the study

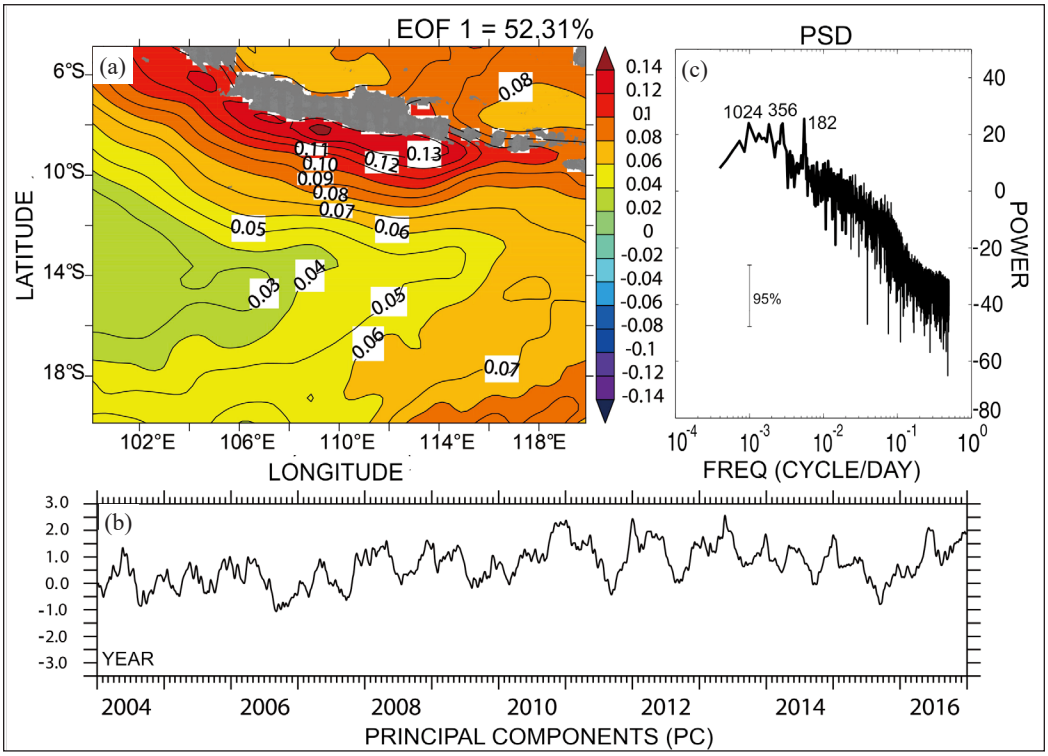

Figure 5. EOF analysis from SLA in the first mode (a) spatial pattern (b) PC graph (c) PSD analysis with 95% of confidence interval

area, especially in the offshore area (Figure 6a). Based on the spatial variation from PC and PSD. Clearly, the fluctuation happened with annual (356 days), inter-annual (1024 days) and semi-annual (186) periodicities (Figure 6b, 6c).

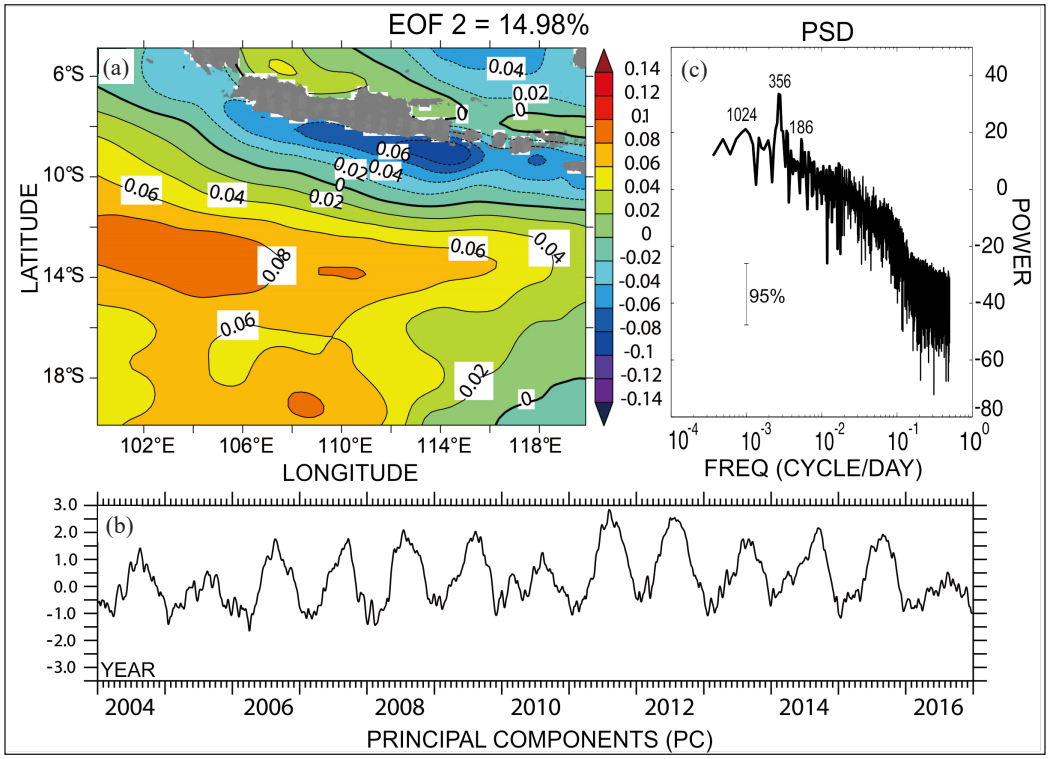

Figure 6. EOF analysis from SLA in the second mode (a) spatial pattern (b) PC graph (c) PSD analysis with 95% of confidence interval

The third and fourth mode were the minor modes, accounting for 7.84% and 4.55% of explained variance, respectively. The third mode, showed in Figure 7, had separated regions of the spatial patterns with negative and positive values. The negative values spread around the coast of Sumatra and Java, and along the western part of the study area. The lowest negative values were seen in Sumatra coast. On the other hand, the positive values spread in the eastern part (Figure 7a). The temporal variation from the PC showed uneven fluctuations. Furthermore, based on the PC and PSD analysis, the variation was clear in being shown as annual (356 days) and semi-annual (182 days) periodicities (Figure 7b, 7c). Subsequently, the fourth mode, presented in Figure 8, showed the spatial pattern with dominant positive values along west coast of Sumatra, spread to offshore heading to the coast of Australia. The negative values were seen in two spots, one around Cilacap coast until Nusa Tenggara, and another one along southwest part of the study area (Figure 8a). The temporal pattern from the PC and PSD showed the dominant fluctuations were annual (356 days) and inter-annual (1024 days) periodicities (Figure 8b, 8c).

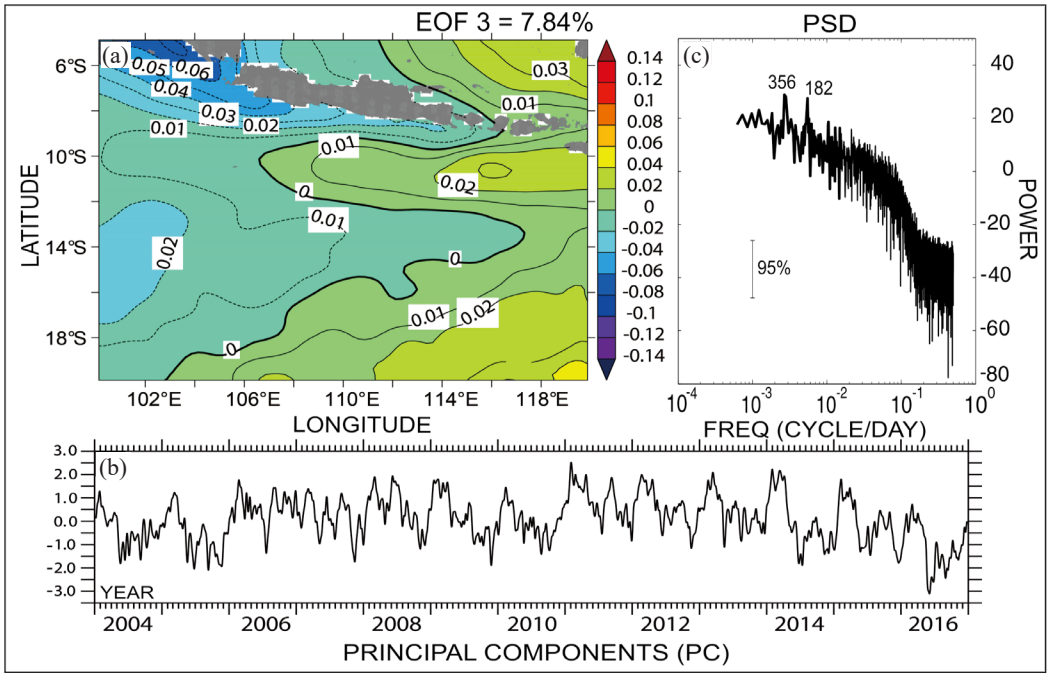

Figure 7. EOF analysis from SLA in the third mode (a) spatial pattern (b) PC graph (c) PSD analysis with 95% of confidence interval

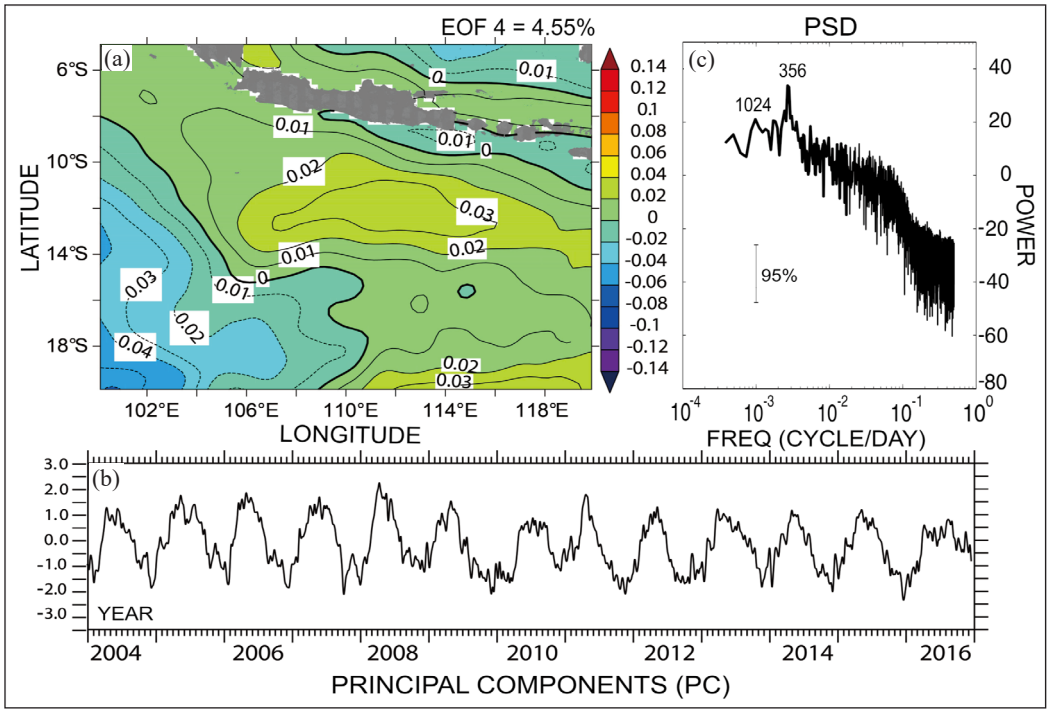

Figure 8. EOF analysis from SLA in the fourth mode (a) spatial pattern (b) PC graph (c) PSD analysis with 95% of confidence interval

The spatial patterns of geostrophic zonal component were interpreted from EOF analysis in the EIO region. Figure 9 showed EOF for geostrophic zonal component to present spatial and temporal patterns of the geostrophic zonal component in the first mode, accounting for 22.27% of the explained variance. For spatial pattern, there was a positive values around the south coast of Java until 12.5°S with the highest positive values lied along west coast of Sumatra, south coast of Java coast until Nusa Tenggara. Right below 12.5°S until the end coverage of the study area was a small variation between negative and positive values (Figure 9a). Temporal fluctuation from PC and PSD analysis in this mode showed that the annual (365 days) periodicity was dominant, followed by semi-annual (182 days) and inter-annual (1024 days) periodicity (Figure 9b, 9c).

The Second EOF mode in zonal geostrophic component was presented in Figure 10, accounting for 6.89% of the explained variance. This mode showed the positive values spreading along the southern Sumatra and Java until Nusa Tenggara coasts with the maximum centered positive values around 106°E-112°E and 8°S-8.5°S. The spatial pattern also showed negative values around 10°S-13°S and the lowest value were centered around 107°E-115°E 11°S-13°S. The contour located below 13°S did not show significant

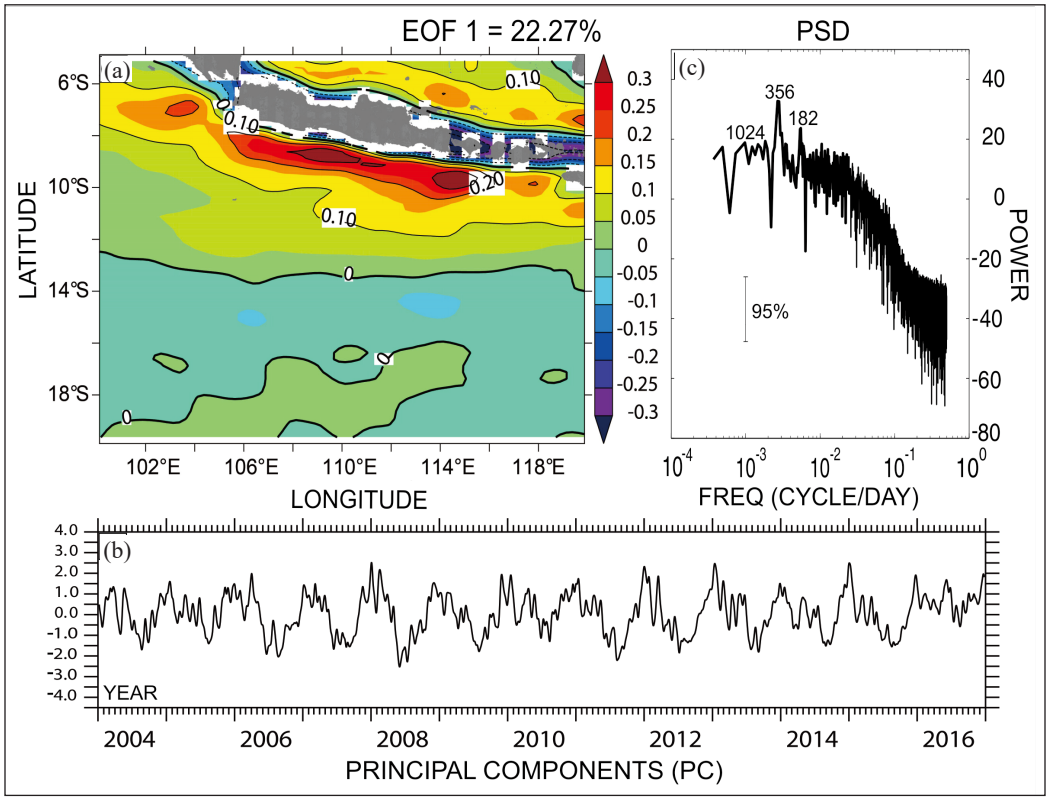

Figure 9. EOF analysis from geostrophic zonal component in the first mode (a) spatial pattern (b) PC graph (c) PSD analysis with 95% of confidence interval

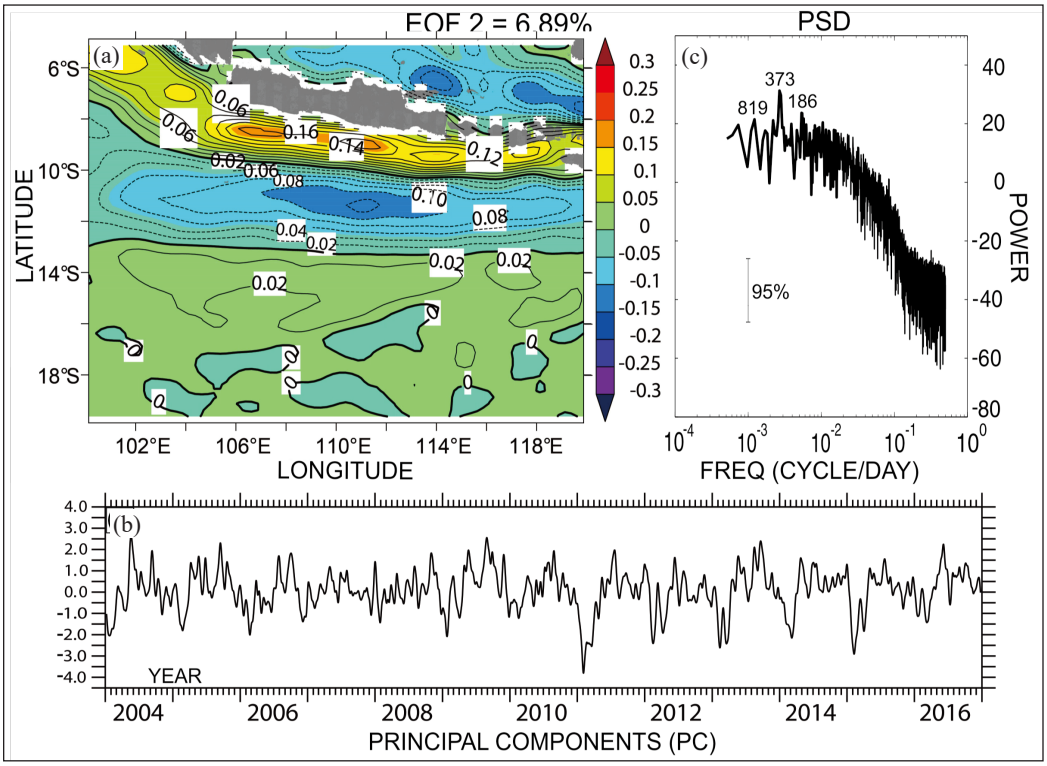

Figure 10. EOF analysis from geostrophic zonal component in the second mode (a) spatial pattern (b) PC graph (c) PSD analysis with 95% of confidence interval

fluctuations (Figure 10a). Temporal variation showed from the PC were annual (373 days), semi-annual (186 days) and inter-annual (819 days) periodicities (Figure 10b, 10c).

The third and fourth mode were minor mode regarding to small number of explained variance. The third mode accounted for 3.6% of the explained variance (Figure 11). The spatial pattern was presented in Figure 11a, showed positive values, seen around the west coast of Sumatra to the south coast of Java, which was almost similar to the second mode. Meanwhile, the negative values were seen around 6°S-10.5°S. Moreover, the rest of the eigenvector values spread along the offshore part of the study area, showing few variations indicated with the small values of positive and negative spatial patterns. The temporal variation from the PC and PSD were observed to be annual (373 days) and semi-annual (186 days) periodicity (Figure 11a, 11b). The fourth mode, accounting for 2.89% of the explained variance (Figure 12), showing the spatial pattern with negative eigenvector around the coast of Sumatra up to 110°E. The negative values were also seen around 100°E-116°E and 10°S-13°S (Figure 12a). Meanwhile, the positive eigenvector values were shown at the eastern part of south Java coast, forming centralization with positive values around 110.5°E -116°E and 9°S-11°S. The temporal variation from the PC and PSD analysis showed annual (372 days) and semi-annual (163 days) periodicities (12b, 12c).

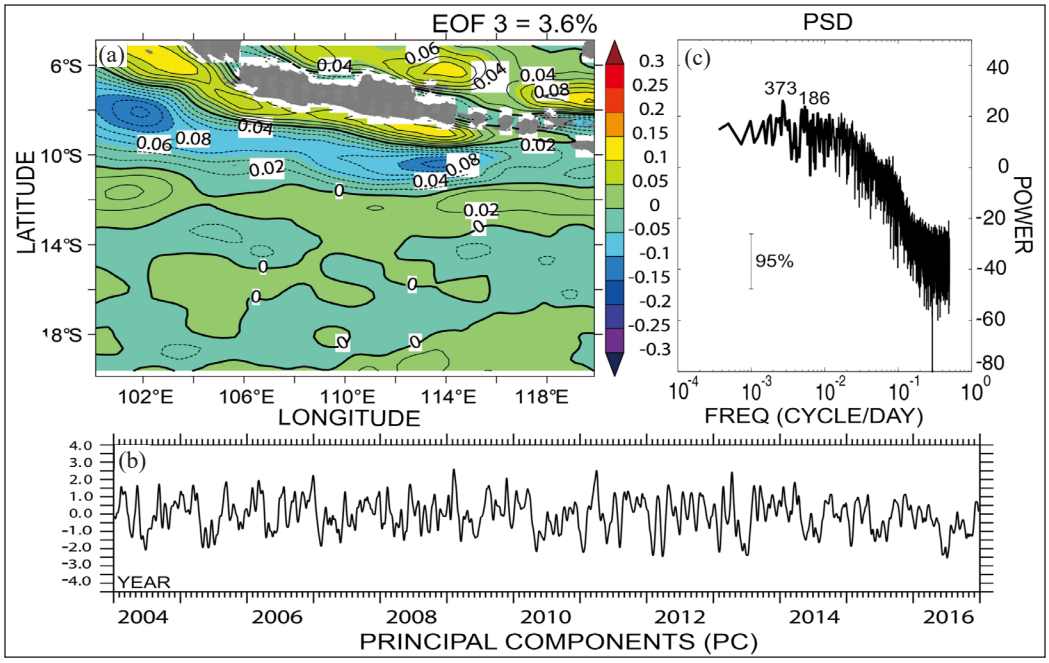

Figure 11. EOF analysis from geostrophic zonal component in the third mode (a) spatial pattern (b) PC graph (c) PSD analysis with 95% of confidence interval

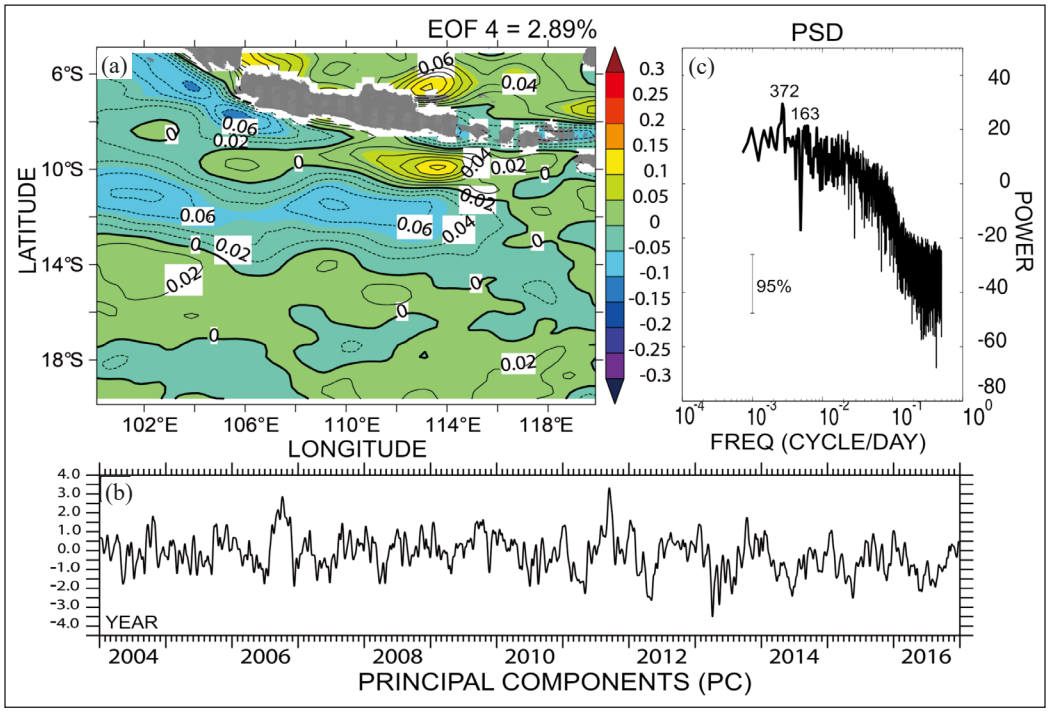

Figure 12. EOF analysis from geostrophic zonal component in the fourth mode (a) spatial pattern (b) PC graph (c) PSD analysis with 95% of confidence interval

The highest standard deviation occurred near the coast of Java both in the SLA and the zonal geostrophic component data (Figures 2b, 2c). Furthermore, there was also a high standard deviation in the area far off Java island. The higher values of standard deviation near the south coast of Java, both in SLA and geostrophic zonal component, might indicate high variability in the area. The highest contour values seen in 111°E-116°E and 8°S-9°S could be affected by Kelvin wave propagation pathway (Clarke & Liu, 1993; Sprintall et al., 2000). The Kelvin wave moves from the equator of the Indian Ocean and causes downwelling near the southern coast of Java. This area is also the pathway of Southeast and northwest monsoon so the area experienced positive-negative anomalies (Susanto et al., 2001). The contour of the minimum standard deviation was seen from the west and east. It might be associated with inter-annual IOD and ENSO phenomena. A more complete descriptions of the area were explained through the results of the EOF analysis.

The results of EOF analysis of SLA from the first to the fourth modes showed variability with semi-annual, annual and inter-annual periodicity. The sum of explained variance was 79.68%. The EOF of SLA in the first mode presented high maximum values along the west coast of Sumatra, the south coast of Java and Nusa Tenggara (Figure 5a). Furthermore, the temporal variation revealed the dominant energy, oscillating in semi-annual, annual and inter-annual periodicity. Special attention was required to analyze the spatial and temporal variations of the SLA in the first mode (Figure 5b,5c). The high positive phase along Sumatra and Java coast might be associated with CTKW that happened semiannually (Sprintall et al., 2000; Syamsudin, 2004). Agreeing with this result, Potemra and Schneider (2007) pointed out that semi-annual Kelvin wave was the large effect of westerly wind bursts during monsoon transition in the Indian Ocean. Sprintall et al. (2000) mentioned that during CTKW, SLA rose along the coast of Sumatra and Java.

Moreover, the temporal variability from PC showed some peaks in April and May, which matched with time series of SLA analysis carried out by Sprintall et al. (2000). The SLA time-series analysis showed that during strong Kelvin wave, the propagation in the monsoon transition period (April-May) was related to the westerly wind bursts. The high SLA signal was associated with equatorial downwelling Kelvin wave propagating eastward, forced by semi-annual westerly wind bursts. Although Kelvin wave propagates semiannually, Wyrtki (1973) said that it would be weaker in the monsoon transition in the October-November period. Syamsudin (2004) pointed out that during 1993-2001, the occurences of Kelvin wave happened either in April-May or November-December. In our results, the occurences of Kelvin wave mostly happened in April-May and November-December, and the weaker November-December Kelvin wave occurred in 2004, 2006, 2009, 2012, 2013 and 2015. Other signals revealed in the first mode's PSD were annual and inter-annual. Although the annual periodicity had been detected in the first mode, based on spatial and temporal variation, it was more significant in the second mode. So, the annual variability of SLA was presented in the second mode.

The SLA variability from second mode was presented in Figure 6. The spatial pattern showed negative values along west coast of Sumatra and south coast of Java while positive values spread in the offshore of southern Java Sea (Figure 6a). The temporal variation also showed the dominant fluctuation's peaks amplitude occurring in July-August-September in the spanning of 2004-2016, and the strongest density energy signal was observed to have annual variation (Figure 6b,6c). Based on that evidence, it could be predicted that the oscillations happening in this mode was influenced by annual monsoon generating upwelling signal. Using the standard deviation of the monthly sea surface temperature, Susanto et al. (2001) revealed annual upwelling along the south coast of Java and west coast of Sumatra. Annual upwelling generated by southeast monsoon happened from June to October. This phenomenon affects colder SST and lower sea level. Another phenomenon that could be seen from this mode was downwelling, happened during northwest monsoon in December-Januari-February, as appeared in the PC's negative peaks.

Inter-annual variability of SLA was seen in the first mode based on temporal variation from PC and correlation coefficient results between the temporal variation of the first mode and IOD index. The correlation coefficient between the IOD index and the first mode of PC from SLA data was -0.41, meaning that there was an inverse correlation between those two variables. During 2004-2016, there were positive (2006, 2012 and 2015) and negative (2010, 2014 and 2016) IOD indexes. In our data, we found the lowest negative anomaly of SLA occurred in 2006. It linked to 2006 positive IOD that consistent with previous study (Horii et al., 2008; Lumban-Gaol et al., 2015). The negative anomaly of SLA in the EIO is occurred when the easterly wind formed in the equator of Indian Ocean, allowing warm pool to move to Africa. Otherwise, we also found the positive anomaly of SLA during negative IOD in 2016. In accordance with Lim & Hendon (2017), the SLA was higher during strong negative IOD in 2016 because the westerly wind intensify, allowing warm pool to concentrate near Indonesia and Australia. Saji et al. (1999) stated that the IOD phenomenon had a powerful influence on the Indian Ocean. Furhermore, Sprintall et al. (2009) found that in 2006, a positive IOD phase coincided by a strong El Niño. In addition, Lim & Hendon (2017) stated, in 2016, there was a strong negative IOD coincided by weak La Niña.

Inter-annual variability in SLA also occurred in ENSO that happened in Pacific Ocean. We found that the variability of SLA experienced a dramatic change when entering the ENSO period. For instance, La-Niña period in 2011, it was seen that the value of PC from SLA data in the first mode showed the highest positive anomaly. The positive anomalies were related to warm pool which was intensively pushed into Indonesia area due to trade wind in equator Pacific Ocean that blew westward during the La-Niña period (Lim & Hendon, 2017). On the other hand, the SLA experienced negative anomaly in 2015, coinciding with El-Niño period. In El-Niño period, the weakening of the trade wind caused

the warm pool to move back into South America, causing SLA around Indonesian seas to be lower. It was consistent with previous studies (Cao et al., 2018; Syamsuddin et al., 2013).

Another variability with lesser contribution showed in the third mode. The spatial pattern in the third mode, accounting for 7.84% of explained variance, got influence from the west area, which might be influenced by the Indian Ocean with negative anomalies. Furthermore, the pattern at the east area might be influenced by the Pacific Ocean with positive anomalies. The temporal variation from the PC graph showed the majority of positive peaks happened in February, March, June, and September. While the negative peaks happened in June, July, and October, November, and December indicated by annual and semi-annual periodicity.

The fourth mode, accounting for 4.55% of explained variance, indicated a different phase of spatial pattern, but not significant. Almost all areas were influenced by positive anomalies. Only two spots were indicated by negative anomalies, around Cilacap and in the southwest of the study area, off the coast. The positive peaks seen from PCs were in April and May, except 2007 that occurred in June, 2010 that occurred in July, and 2016 that occurred in September. While the negative peaks mostly happened in October, November, and December. Except in 2006 and 2016 which was in January. The dominant periodicity that occurred in this area was annual variability.

The spatio-temporal variability of geostrophic zonal component was described in the highest four-modes, accounted for 36.65% of cummulative explained variance. It was far from the threshold of determining how many modes would be used provided by Jolliffe (2002), but it was not possible to use more modes, because the explained variance percentage was getting smaller for the fifth mode and forward. This means that it was not possible to explain spatial and temporal variability from a small percentage of explained variance (<2.89%). So only the highest four-modes were included in this study to make it consistent with SLA modes.

The spatial pattern of the geostrophic zonal component in the three leading EOF showed positive values around Sumatra and Java coast as showed in Figure 9a, 10a, and 11a, respectively. In the spatial pattern of the first mode, there was positive values along the west coast of Sumatra-the south coast of Java, centralized around the south coast of Java. Referring to the annual period of the variability, it was suspected to be annual upwelling. It occurred during the southeast monsoon that flowed westward, removing light surface water and generating upwelling along Java coast (Fieux et al., 1996). Hence, water circulation flows westward. During monsoon transition, westerly wind forces from the equatorial Indian Ocean, generating Kelvin wave with the semi-annual period (Sprintall et al., 2000). The semi-annual signal was shown in several years in the PC, for example, in April 2004 and May 2005. Besides that, the inter-annual variability in this mode leads to some arguments. Chen, et al. (2016) argued that inter-annual variability in the equatorial EIO is upwelling and

closely associated with IOD, while a few were associated with the ENSO event. Regarding the ENSO, it was reported that the ITF was higher during La Niña than El-Niño (Meyers, 1996). On the other hand, Sprintall et al., (2009) found that the surface ITF anomaly was strong during positive IOD coinciding with strong El-Niño in 2006.

The second mode showed positive values along Sumatra and Java coast, and the typical pattern was considered as the SJC pathway (Figure 10a). The SJC is generated by local wind stress along the coast of Sumatra and Java and part of the easterly semi-annual equatorial jet reflection generated in central Indian Ocean during monsoon transition (Clarke & Liu, 1993; Meyers et al., 1995). The maximum eastward SJC flows in May and November (Bray et al., 1997). The negative values, seen around 10°S-13°S, was the same location with the SEC region, that was consistent with previous study (Feng & Wijffels, 2002). The SEC annually flows from ITF, where it is transported to the EIO that flows westward, carrying a mass of water with low salinity. The highest intensity of the geostrophic component in the SEC was in July-November, and the weak energy transport happened when the eastward SJC strengthened (Bray et al., 1997; Feng & Wijffels, 2002; Meyers et al., 1995).

The third and fourth modes contributed very little variability, with 3.6% and 2.89% of explained variance. In the third mode, there was a spatial pattern with positive anomalies near the west coast of Sumatra and South of Java, while the negative anomalies were around 6°S-10.5°S. The spatial pattern was similar to the second mode, it might be associated with SJC and SEC propagation path. The temporal variation of the PC showed positive peaks in February, March, September, November, and December with annual, semi-annual and seasonal periodicity. Whereas in the fourth mode, although it had positive and negative anomalies with a number of centralization, the variation was not significant. The temporal period oscillated in January, February, September, and October, and negative peaks were in May, April, and July. The variability oscillated in annual, inter-annual and semi-annual periodicity.

CONCLUSION

The investigation result of SLA and geostrophic zonal component showed great variations near the south coast of Java. The spatial pattern of SLA in the first mode was dominated by positive eigenvector with the high value around Sumatra and Java coast, while the second mode showed negative values around Sumatra and Java coast, and positive values along the offshore region, while the third and the fourth mode did not show a substantial spatial variability. The temporal variability results showed semi-annual, annual and inter-annual periodicity. Based on the spatial and temporal patterns of SLA data, it was suspected that SLA variability that occurred in the EIO region might be associated with semi-annual Kelvin wave, annual upwelling, and inter-annual IOD and ENSO phenomena.

Furthermore, the EOF analysis for geostrophic zonal component in the first mode showed that there were positive values around Sumatra and Java coast, while negative value spread along the offshore region. In the second mode, the spatial pattern showed positive values near the coastal area, and negative values around 10°S-13°S, with annual, semi-annual and inter-annual periodicity. In the third and the fourth mode, the spatial pattern showed low variability. The dominant temporal variation revealed annual, semi-annual and inter-annual periodicity. It was also suspected that spatial and temporal variability in the geostrophic zonal component was supposed to be upwelling, Kelvin wave, and the ITF during IOD and ENSO. It was noticed that some patterns could be associated with the SJC and SEC signals.

ACKNOWLEDGMENT

This study has been conducted using E.U Copernicus Marine Service Information. The authors would also like to express their special gratitude to the colleagues at Marine Technology major, the Oceanographic Data Processing Laboratory and colleagues at the Oceanographic Physics Laboratory of IPB University for their suggestions and input for the sake of accomplishing this research.

REFERENCES

Atmadipoera, A. S., Horhoruw, S. M., Purba, M., & Nugroho, D. Y. (2016). Spatial and temporal variation of Indonesian Throughflow in the Makassar Strait. *Ilmu Dan Teknologi Kelautan Tropis*, *8*(1), 299-320.

AVISO. (2016). *SSALTO/DUACS User Handbook : MSLA and (M)ADT Near-Real Time and Delayed Time Products*. France (FR): CNES.

Björnsson, H., & Venegas, S. (1999). *A Manual for EOF and SVD analyses of climatic data*. Montreal, Canada: McGill University.

Bray, N. A., Wijffels, S. E., Chong, J. C., Fieux, M., Hautala, S., Meyers, G., & Morawitz, M. L. (1997). Characteristics of the Indo-Pacific throughflow in the eastern Indian Ocean. *Geophysical Research Letters*, *24*(21), 2569-2572.

Cao, G. J., He, Y. J., Wei, Z. X., & Xu, T. F. (2018). Interannual modulation of intraseasonal sea level variability along the southern coast of Java. *Science China Earth Sciences*, *61*(1), 1-12.

Chen, G., Han, W., Li, Y., & Wang, D. (2016). Interannual variability of Equatorial Eastern Indian Ocean upwelling : Local versus remote forcing. *Journal of Phisical Oceanography*, *46*, 789-807.

Clarke, A. J., & Liu, X. (1993). Observations and dynamical of semiannual and annual sea levels near the eastern equatorial indian ocean boundary. *Journal of Physical Oceanography*, *23*, 386-399.

Escudier, P., Couhert, A., Mercier, F., Mallet, A., Thibaut, P., Tran, N., ... & Ablain, M. (2017). *S*atellite altimeter over ocean and land surfaces. In D. Stammer & A. Cazenave (Eds.), *Satellite altimetry over oceans and land surfaces* (pp. 1-70). Boca Raton, Florida: CRC Press.

Fang, W., Guo, J., Shi, P., & Mao, Q. (2006). Low frequency variability of South China Sea surface circulation from 11 years of satellite altimeter data. *Geophysical Research Letters*, *33*(22), 1-5.

Feng, M., & Wijffels, S. (2002). Intraseasonal variability in the SEC of the East Indian ocean. *Journal of Geophysical Research*, *32*, 265-277.

Fieux, M., Molcard, R., & Ilahude, A. G. (1996). Geostrophic transport of the Pacific-Indian Oceans throughflow. *Journal of Geophysical Research*, *101*(95), 12421-12432.

Fitrianah, D., Hidayanto, A. N., Lumban-Gaol, J., Fahmi, H., & Arymurthy, A. M. (2016). A spatio-temporal data-mining approach for identification of potential fishing zones based on oceanographic characteristics in the Eastern Indian Ocean. *IEEE Journal of Selected Topics in Applied Earth Observations and Remote Sensing*, *9*(8), 3720-3728.

Fu, L. L., & Cazenave, A. (2001). *Satellite altimetry and earth sciences*. San Diego, California: Academic Press.

Fu, L. L., & Chelton, D. B. (1985). Observing large-scale temporal variability of ocean currents by satellite altimetry: With application to the Antarctic circumpolar currents. *Journal of Geophysical Research*, *90*(C3), 4721-4739.

Gill, A. E. (1982). *Atmosphere-ocean dynamics*. New York, NY: Academic Press.

Gordon, A., & Kamenkovich, V. (2010). "Modeling and observing the Indonesian Throughflow " a special issue of dynamics of atmosphere and ocean. *Dynamic of Atmospheres and Ocean*, *50*, 113-114.

Hannachi, A. (2004). *A Primer for EOF analysis of climate data* (pp. 1-33). England, UK: University of Reading.

Hannachi, A., Jolliffe, I. T., & Stephenson, D. B. (2007). Empirical orthogonal functions and related techniques in atmospheric science: A review. *International Journal of Climatology*, *27*(December 2007), 1549-1555.

Horii, T., Hase, H., Ueki, I., & Masumoto, Y. (2008). Oceanic precondition and evolution of the 2006 Indian Ocean dipole. *Geophysical Research Letters*, *35*(3), 1-6.

Izumo, T., Vialard, J., Lengaigne, M., de Boyer Montegut, C., Behera, S. K., Luo, J. J., … & Yamagata, T. (2010). Influence of the state of the Indian Ocean Dipole on the following years El Nĩno. *Nature Geoscience*, *3*(3), 168-172.

Jolliffe, I. T. (2002). *Principal component analysis, Second Edition*. New York, NY: Springer-Verlag.

Joseph, A. (2014). *Measuring ocean currents: Tools, technologies, and data* (1st Ed.). Waltham, MA: Elsevier.

Le Traon, P. Y. (2013). From satellite altimetry to Argo and operational oceanography : three revolutions in oceanography. *Ocean Science*, *9*(5), 901-915.

Lim, E., & Hendon, H. H. (2017). Causes and predictability of the negative Indian Ocean Dipole and its impact on La Niña During 2016. *Nature*, (June), 1-11.

Liu, Y., & Weisberg, R. H. (2007). Ocean currents and sea surface heights estimated across the West Florida Shelf. *Journal of Physical Oceanography*, *37*(6), 1697-1713.

Lumban-Gaol, J., Leben, R. R., Vignudelli, S., Mahapatra, K., Okada, Y., Nababan, B., … & Syahdan, M. (2015). Variability of satellite-derived sea surface height anomaly, and its relationship with Bigeye tuna (Thunnus obesus) catch in the Eastern Indian Ocean. *European Journal of Remote Sensing*, *48*, 465-477.

Mansawan, A. A., Lumban-Gaol, J., & Panjaitan, J. P. (2016). Variation and trend of sea level derived from altimetry satellite and tide gauge in cilacap and benoa coastal areas. *International Journal of Remote Sensing and Earth Sciences*, *13*(1), 59-66.

Meyers, G. (1996). Variation of Indonesian throughflow and the El Nino - Southern Oscillation. *Science China Earth Sciences*, *101*(95), 12255-12263.

Meyers, G., Bailey, R. J., & Worby, A. P. (1995). Geostrophic transport of Indonesian throughflow. *Deep-Sea Research Part I*, *42*(7), 1163-1174.

Pond, S., & Pickard, G. L. (1983). *Introductory dynamical oceanography* (2nd Ed.). Oxford, England: Butterworth-Heineann Ltd.

Potemra, J. T., & Lukas, R. (1999). Seasonal to interannual modes of sea level variability in the western Pacific and eastern Indian oceans. *Geophysical Research Letters*, *26*(3), 365-368.

Potemra, J. T., & Schneider, N. (2007). Interannual variations of the Indonesian throughflow. *Journal of Geophysical Research: Oceans, 112*(C5), 1-13.

Rahmawitri, H., Atmadipoera, A. S., & Sukoraharjo, S. S. (2016). Circulation and current variability in the Sunda Strait waters. *Jurnal Kelautan Nasional*, *11*(3), 141-157.

Rosmorduc, V., Benveniste, J., Bronner, E., Dinardo, S., Lauret, O., Maheu, C., … & Picot, N. (2011). *Radar Altimetry Tutorial*. Howard Place, South Africa: CSL Publisher.

Saji, N. H., Goswami, B. N., Vinayachandran, P. N., & Yamagata, T. (1999). A dipole mode in the tropical Indian Ocean. *Nature*, *401*, 360-363.

Schiller, A., Wijffles, S., Sprintall, J., Molcard, R., & Oke, P. (2009). Pathways of intraseasonal variability in the Indonesian throughflow region. *Dynamics of Atmospheres and Oceans, 50*(2), 174-200.

Schott, F. A., Xie, S. P., & McCreary-Jr, J. P. (2009). Indian Ocean circulation and climate variability. *Reviews of Geosphisics*, *47*(RG1002), 1-46.

Song, Q., Gordon, A., & Visbeck, M. (2004). Spreading of the Indonesian throughflow in the Indian Ocean. *Journal of Physical Oceanography*, *34*, 772-792.

Sprintall, J., Gordon, A., Murtugudde, R., & Susanto, R. D. (2000). A semiannual Indian Ocean forced Kelvin wave observed in the Indonesian seas in May 1997. *Journal of Geophysical Research*, *105*, 17217-17230.

Sprintall, J., Wijffels, S. E., Molcard, R., & Jaya, I. (2009). Direct estimates of the Indonesian Throughflow entering the Indian Ocean : 2004 – 2006. *Journal of Geophysical Research*, *114*(C07001), 1-19.

Sprintall, J., Wijffels, S., Molcard, R., & Jaya, I. (2010). Direct evidence of the South Java Current system in Ombai Strait. *Dynamics of Atmospheres and Oceans*, *50*(2), 140-156.

Stewart, R. H. (2008). *Introduction to Physical Oceanography*. Texas, USA: Texas A & M University.

Susanto, R. D., Ffield, A., Gordon, A., & Adi, T. R. (2012). Variability of Indonesian throughflow within Makassar Strait , 2004-2009. *Journal of Geophysical Research*, *117*(C09013), 2004-2009.

Susanto, R. D., Gordon, A., & Zheng, Q. (2001). Upwelling along the coasts of Java and Sumatra and its relation to ENSO. *Geophysical Research Letters*, *28*(8), 1599-1602.

Susanto, R. D., & Song, Y. (2015). Indonesian throughflow proxy from satellite altimeters and gravimeters. *Journal of Geophysical Research : Oceans*, *120*, 2844-2855.

Syah, A. F., Saitoh, S. I., Alabia, I. D., & Hirawake, T. (2016). Predicting potential fishing zones for pacific saury (Cololabis saira) with maximum entropy models and remotely sensed data. *Fishery Bulletin*, *114*(3), 330-342.

Syamsuddin, M. L., Saitoh, S. I., Hirawake, T., Samsul, B., & Harto, A. B. (2013). Effects of El Niño-Southern Oscillation events on catches of Bigeye Tuna (Thunnus obesus) in the eastern Indian Ocean off Java. *Fishery Bulletin*, *111*(2), 175-188.

Syamsudin, F. (2004). Semiannual Kelvin Waves Propagation along the South Coast of Sumatra-Jawa-Bali and the Lesser Sunda Islands observed by TOPEX / POSEIDON and ERS-1 / 2 Satellites. *Journal of Engineering and Technological Sciences*, *36*(2), 133-139.

Syamsudin, F., & Kaneko, A. (2013). Ocean variability along the southern coast of Java and Lesser Sunda Islands. *Journal of Oceanography, 69*(5), 557-570.

Thomson, R. E., & Emery, W. J. (2014). *Data analysis method in physical oceanography* (3rd Ed.). Amsterdam, The Netherlands: Elsevier.

Tomczak, M., & Godfrey, J. S. (2001). *Regional oceanography: An introduction* (1.0). London, UK: Elsevier.

Trauth, M. H. (2014). *MATLAB ® Recipes for earth sciences* (4th Ed.). Berlin, Germany: Springer.

Wyrtki, K. (1961). *NAGA REPORT, Scientific result of marine investigaitons of the South China Sea and the Gulf of Thailand 1959-1961* (Vol. 2). University of California, Scripps Institution of Oceanography, California.

Wyrtki, K. (1973). Physical oceanography of the Indian Ocean. In B. Zeitzschel & S. A. Gerlach (Eds.), *The biology of the Indian Ocean* (Vol. 3, pp. 18-23). Berlin, Germany: Springer.